nature materials

Article

https://doi.org/10.1038/s41563-026-02561-2

Removing aluminium impurities in primary magnesium at an ultra-low cost

Received: 6 February 2025

Accepted: 2 March 2026

Published online: 3 April 2026

Check for updates

Rui Zheng, Bo Yang, Yue-Cun Wang, Bo-Yu Liu, Wei-Yi Yang & Zhi-Wei Shan

The content of aluminium impurity in primary magnesium produced via silicothermic reduction often fluctuates uncontrollably. Such variability harms the market credibility and economic performance of producers, as well as constraining the material's suitability for certain high-end applications. Existing purification methods are either inefficient or prohibitively expensive. Inspired by the frequent detection of Ca–Al–F–O compounds in troublesome deposits formed during the reduction process, we propose using CaO to trap aluminium impurities in magnesium vapour, where it reacts with AlF to form $Ca_{12}Al_{14}F_2O_{32}$, as supported by thermodynamic calculations. By constructing a miniaturized silicothermic reduction apparatus in our laboratory, we show that CaO can reduce aluminium impurities in magnesium down to 6.3 ppm, achieving over 90% removal efficiency. In industrial-scale applications, by using calcined dolomite—a cost-effective, readily available raw material in magnesium plants—the percentage of primary magnesium with aluminium impurities satisfying the Mg9998 grade could be raised from nearly zero to 83%. Compared with the current most popular high-purity magnesium production technology, our approach lowers extra purification costs by ~96%, enabling large-scale, ultra-low-cost production of high-purity magnesium with low aluminium.

Magnesium and its alloys, owing to their exceptional properties such as high strength-to-weight ratio, strong reducing ability, excellent biocompatibility and biodegradability, hold tremendous potential for a wide range of advanced applications in lightweight transportation, strategic metal reduction and biodegradable implants[1–4]. Nowadays, approximately 80% of the world's primary magnesium is produced by the silicothermic reduction process[5,6], which is cost-effective and suitable for large-scale production. However, primary magnesium produced by this method often contains unwanted impurities, which compromise its desirable properties, economic value and performance in critical applications[7,8]. Among metallic impurities in primary magnesium, aluminium is particularly problematic due to its higher concentrations and larger fluctuations than other elements[9] (a trend also seen in Supplementary Fig. 1). Such excess and variability not only restrict efforts to upgrade primary magnesium, causing profit losses (Supplementary Notes 1 and 2) but also destabilize downstream processing, compromise material reliability and limit its use in high-end applications. Typical cases are titanium and zirconium production, where magnesium widely serves as the reductant[4,10]. For sputtering targets, ASTM F-1709-16 requires titanium of ≥99.99% purity. Yet aluminium impurity is especially difficult to eliminate in post-purification steps (for example, through molten salt electrorefining[11,12] or electron-beam refining[13]) due to its electrochemical similarity and strong affinity with titanium. It has been reported that the production of semiconductor-grade titanium requires sponge titanium with aluminium impurity levels of ≤50 ppm (ref. 14), and achieving <1-ppm aluminium impurity in final titanium necessitates sponge titanium containing <10-ppm aluminium[9]. Since magnesium has been identified as the primary aluminium source in

Engineering Research Center for Magnesium-based New Materials, Center for Advancing Materials Performance from the Nanoscale (CAMP-Nano), State Key Laboratory for Mechanical Behavior of Materials, Xi'an Jiaotong University, Xi'an, China. e-mail: zwshan@mail.xjtu.edu.cn

https://doi.org/10.1038/s41563-026-02561-2

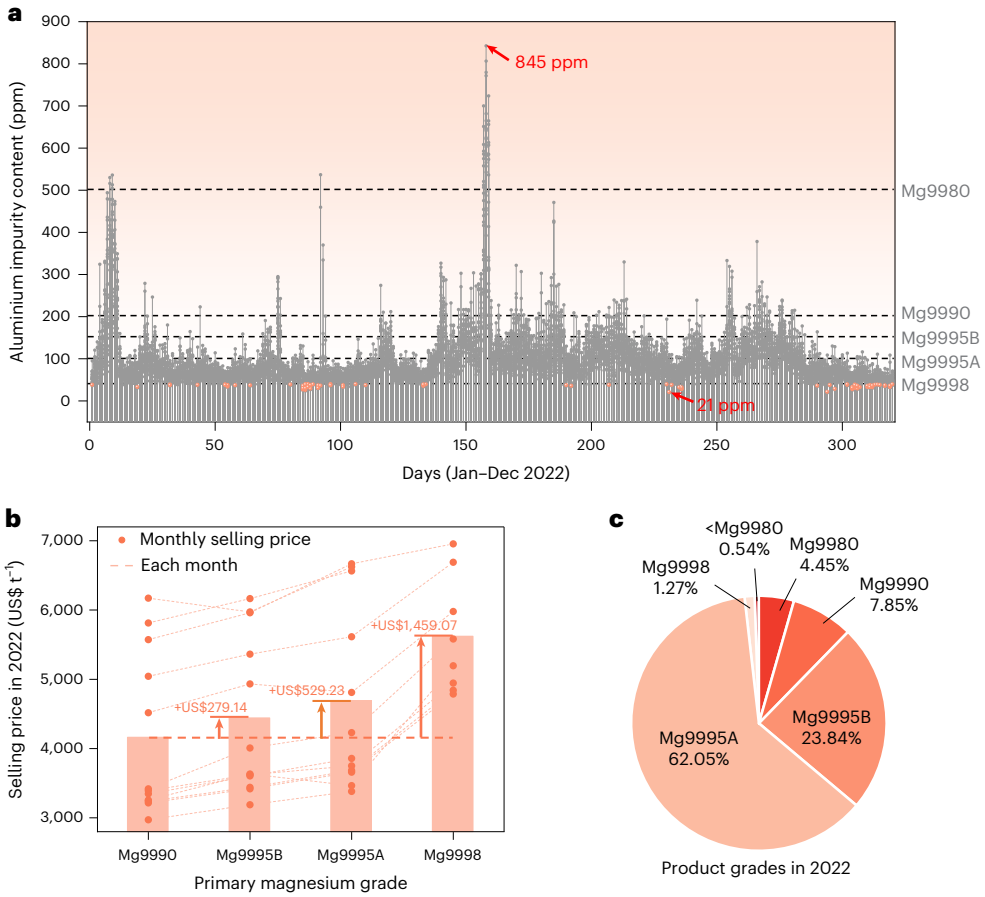


Fig. 1 | Aluminium impurity content fluctuations in magnesium and the resulting economic impact. a, Aluminium impurity levels in magnesium ingots produced by a leading manufacturer in 2022. Each column represents the aluminium content of all production batches on a specific day, with each point corresponding to an individual production batch weighing approximately 2 t. The aluminium content fluctuated substantially, with a peak of 845 ppm, more than 32 times that of the lowest level (21 ppm), spanning five purity grades as defined by ISO 8287:2021. **b**, Selling prices of different magnesium grades in 2022. Bars indicate the average monthly selling price, and dots represent the selling price in each individual month (Mg9990, $n = 12$; Mg9995B, $n = 8$; Mg9995A, $n = 12$; Mg9998, $n = 7$). n reflects the number of months in which each grade was actually sold, as some grades were not traded in certain months; months without sales were not included in the averaging. Mg9995B and Mg9995A achieved premiums of US$279–529 t^{-1} over Mg9990, the mainstream industry standard, whereas Mg9998 commanded a much higher premium of US$1,459 t^{-1}. **c**, Despite the aluminium impurity content in magnesium meeting the requirements of Mg9995B and Mg9995A grades for the majority of production, there still existed 1.27% of the products with aluminium impurity content satisfying the Mg9998 grade.

sponge titanium[7,15,16], strict aluminium control in primary magnesium is indispensable. A comparable requirement exists in nuclear-grade zirconium production, where the allowable aluminium content in magnesium reductant is typically restricted to ≤50 ppm (Supplementary Note 3). This is because even trace aluminium can markedly deteriorate the corrosion resistance of zirconium and its alloys in high-temperature water and steam environments, particularly in the presence of other impurities[17–19]. In biomedical applications[20–23], aluminium impurity is also undesirable: it is neurotoxic[24] and markedly accelerates corrosion. For instance, increasing aluminium impurity content in pure magnesium from 28.5 ppm to 81.5 ppm can lead to an approximately 3.5-fold rise in corrosion rate (Supplementary Fig. 2). In addition, in nominally aluminium-free magnesium alloys, especially Mg–Zr systems, aluminium is widely recognized as a highly sensitive impurity that degrades the effectiveness of costly Zr-based grain refiners[25,26]. Collectively, these considerations underscore the critical necessity of controlling aluminium impurities in magnesium.

Flux refining[27–29] and vacuum distillation[30–33] are the two most common methods for magnesium purification. Flux refining can remove reactive metal impurities (for example, K, Ca and Na) and metal oxides by forming a sludge of heavy oxychlorides for separation on settling[27,34]. However, it has a fairly limited effect in removing aluminium and other metal impurities in magnesium. Vacuum distillation[30–33] is the most effective technique to produce high-purity magnesium, but it is energy-intensive and costly: it requires reheating primary magnesium for distillation purification, and the higher the desired purity, the lower the distillation efficiency[7]. Consequently, high-purity magnesium produced by the vacuum distillation process is usually prohibitively expensive for most industrial applications. Most recently, Yang et al.[9] reported an effective way to reduce aluminium impurities in the early stage of primary magnesium production. They found fluorite (CaF_2, a catalyst used to foster the silicothermic reduction process[35,36]) can transform Al or Al_2O_3 in feedstocks into gaseous AlF, making AlF the primary form of aluminium impurity in magnesium vapour[9]. Due to its similar vapour pressure to magnesium, AlF is prone to co-condense with magnesium vapour and contaminate the magnesium[9]. Although reducing or eliminating the use of fluorite can suppress the formation of AlF and substantially lower aluminium impurities in primary magnesium, this fluorite-free method also decreases the production efficiency and substantially raises production costs. Moreover, despite the identification of AlF as the primary carrier of aluminium, no cost-effective method has yet been developed to reliably suppress aluminium contamination in primary magnesium, underscoring the urgent need for new, economically viable strategies.

https://doi.org/10.1038/s41563-026-02561-2

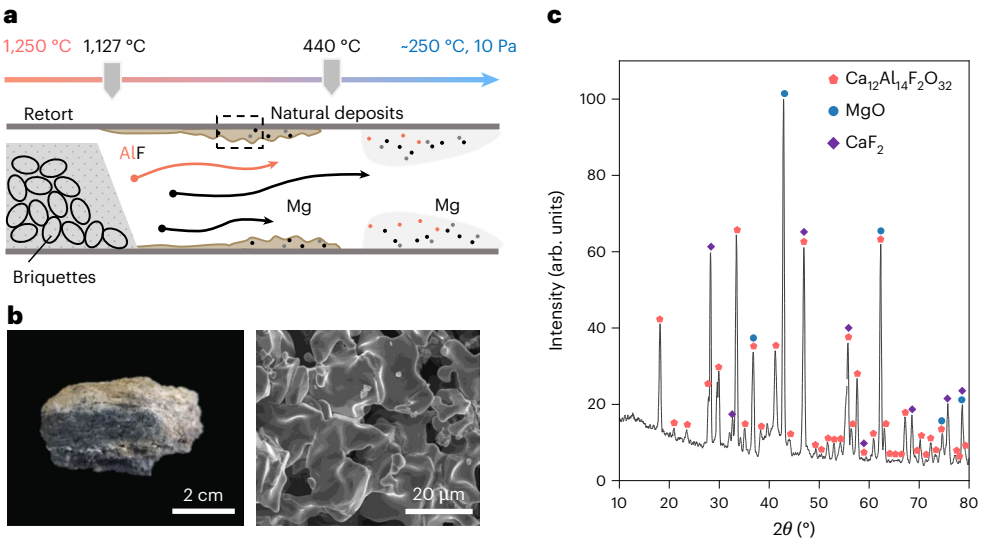


Fig. 2 | Predeposition of aluminium impurities from magnesium vapour as natural deposits. a, Schematic of the silicothermic reduction process, illustrating the temperature gradient and the formation of natural deposits in the retort. Magnesium vapour forms from briquettes at high temperatures and condenses into crystals in the cooling zone. Several natural deposits form in the temperature range of 1,127 °C–440 °C. **b**, Macroscopic image (left) and SEM image (right) of natural deposits. **c**, XRD analysis of the deposits, confirming the presence of aluminium-containing $Ca_{12}Al_{14}F_2O_{32}$ phase, along with the CaF_2 and MgO phases.

Results

Impurity removal mechanism inspired by the troublesome deposit analysis

To understand the extent and fluctuation of aluminium impurities in primary magnesium, the composition data at a leading magnesium plant, which is known for the quality of their magnesium product, was analysed. This plant has an annual production capacity of 30,000 t. The aluminium impurity levels in 2022 exhibited unexpectedly large fluctuations. As shown in Fig. 1a, each column represents the aluminium content in ingots produced on a single day, with each data point corresponding to a production batch of ~2 t. The aluminium content ranged from 21 ppm to 845 ppm, with the highest value being over 32 times that of the lowest. Moreover, the aluminium content crosses five purity grades as specified by ISO 8287:2021 (Mg9980, Mg9990, Mg9995B, Mg9995A and Mg9998), where Mg9998 represents the highest purity here.

The cost or selling price of magnesium products usually correlates strongly with the purity grade. According to the real sales data in 2022 (Fig. 1b), Mg9995B and Mg9995A fetch premiums of US$279.14 to US$529.23 t^{-1} over Mg9990, the most common grade on the market. Mg9998 commands a notably higher premium of US$1,459.07 t^{-1}. The distribution of purity grades in primary magnesium can directly impact the economic benefits for the producer (Supplementary Note 2). As summarized in Fig. 1c, when only considering aluminium impurity levels—the primary factor limiting magnesium grading (Supplementary Fig. 1)—62.05% of the magnesium meets the Mg9995A grade and 23.84% meets the Mg9995B grade. However, the aluminium impurity contents that satisfy the requirement for Mg9998 grade (corresponding to an aluminium impurity content of ≤40 ppm, ISO 8287:2021) are of particular interest. As shown in Fig. 1c, Mg9998 accounts for approximately 1.27% of the total production (Fig. 1a, orange data points). Typically, achieving such low aluminium impurity levels for Mg9998 grade requires additional vacuum distillation[35,37]. The existence of the small amount of Mg9998 suggests that the current silicothermic reduction process is likely to produce magnesium with aluminium impurity levels that meet the Mg9998 grade, provided the key parameters are identified. In other words, by determining these key parameters, the yield of Mg9998-grade magnesium can be raised substantially in the existing silicothermic reduction process with minimal additional cost.

To identify the key factors influencing the aluminium impurity levels in primary magnesium, the data shown in Fig. 1a were carefully analysed. The fluctuations are often observed within a single day or over a few adjacent days, exhibiting sharp peak-like patterns. As mentioned above, primary magnesium is the product obtained after refining crude magnesium, and crude magnesium is the direct product of the reduction process. On the basis of the fundamental principles of the refining process, it is unlikely to be the source of these substantial fluctuations. Therefore, the investigation was focused on the production of crude magnesium, that is, the reduction process.

As shown in Fig. 2a, the briquettes composed of calcined dolomite (CaO·MgO), ferrosilicon and fluorite are placed in a vacuum reduction retort. Under conditions of ~1,250 °C and ~10-Pa vacuum, ferrosilicon reacts with CaO·MgO to generate gaseous magnesium, impurities and solid dicalcium silicate slag. Driven by pressure and temperature gradients, magnesium and impurity atoms flow towards the lower-temperature crystallization zone, where magnesium and impurities condense into crude magnesium. Since the briquette composition and operational conditions are unlikely to vary markedly within a single day, the daily aluminium impurity levels would be expected to remain relatively stable. The observed single-day fluctuations (Fig. 1a and Supplementary Fig. 1b) are, therefore, probably attributed to factors occurring between the generation of magnesium vapour and its crystallization.

It can be found that some troublesome deposits often form on the inner wall of the retort during the silicothermic reduction process (Fig. 2a). These deposits must be cleaned regularly, otherwise heat transfer efficiency decreases and consequently reduces the output of crude magnesium[38]. Deposit samples from different locations of the retort have different colours (Supplementary Fig. 3b). A brownish compound with its surface exhibiting a porous structure attracted our attention (Fig. 2b). This compound was generated over a wide temperature range of 1,126.7 °C–439.7 °C (Supplementary Fig. 3a). X-ray diffraction (XRD) analysis revealed that the brownish deposit predominantly consists of a high-aluminium $Ca_{12}Al_{14}F_2O_{32}$ phase together with MgO and CaF_2 (Fig. 2c). This finding suggests that the formation of these

https://doi.org/10.1038/s41563-026-02561-2

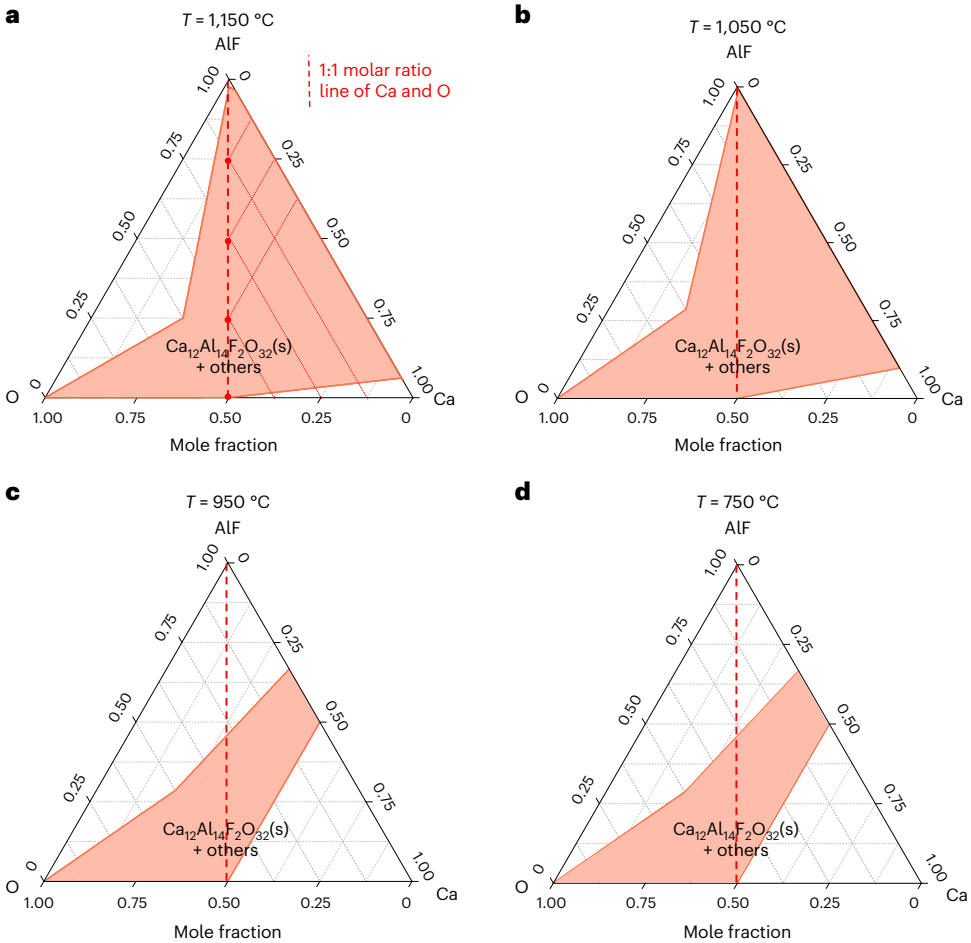


Fig. 3 | Thermodynamic calculation of the possibility of forming $Ca_{12}Al_{14}F_2O_{32}$ deposits. a–d, Ternary phase diagrams of the AlF–Ca–O system at 10 Pa, illustrating the formation regions of $Ca_{12}Al_{14}F_2O_{32}$ at different temperatures: (**a**) 1,150 °C, (**b**) 1,050 °C, (**c**) 950 °C and (**d**) 750 °C. The orange areas represent the zones containing solid $Ca_{12}Al_{14}F_2O_{32}$, and other phases are detailed in Supplementary Note 6. Across **a**–**d**, $Ca_{12}Al_{14}F_2O_{32}$ remains formable over a broad temperature range, but its formation region varies notably with temperature. From 1,150 °C to 1,050 °C and from 950 °C to 750 °C, the proportion of the orange area changes only slightly. By contrast, when the temperature decreases from 1,050 °C to 950 °C, the $Ca_{12}Al_{14}F_2O_{32}$ phase zone diminishes markedly, indicating a reduced formation likelihood below 950 °C. Interestingly, at high temperatures, when the molar ratio of Ca to O is 1:1 (marked by the red dashed line), $Ca_{12}Al_{14}F_2O_{32}$ is always prone to form, regardless of the molar percentage of AlF.

aluminium-rich deposits may be linked to fluctuations in aluminium impurity levels and could offer insights into optimizing conditions for lowering aluminium impurities.

Our previous work has demonstrated that aluminium impurities in magnesium vapour mainly exist in the form of gaseous AlF (ref. 9). In addition, previous studies[9,34,39–41] showed that the gaseous substances produced during the silicothermic reduction process can contain calcium atoms and gaseous SiO, which can serve as the source of oxygen. On the basis of this, it is reasonable to speculate that Ca and O play a critical role in capturing gaseous AlF, thereby influencing the formation of $Ca_{12}Al_{14}F_2O_{32}$.

Theoretical insights into the impurity removal mechanism

To validate the above hypothesis, the ternary phase diagram of AlF–Ca–O was calculated at different temperatures (Fig. 3). The orange-shaded regions represent the compositional conditions under which the $Ca_{12}Al_{14}F_2O_{32}$ substance can be formed at the given temperature and pressure. Other phases are detailed in Supplementary Fig. 5. Obviously, the areas of the orange regions decrease as the temperature drops, indicating that lower the temperature, the stricter the requirements for the AlF, Ca and O ratios to form $Ca_{12}Al_{14}F_2O_{32}$. However, the extent of this reduction varies markedly with temperature. For instance, when the temperature drops from 1,150 °C to 1,050 °C (Fig. 3a,b) as well as from 950 °C to 750 °C (Fig. 3c,d), the proportion of the orange area changes only slightly. By contrast, when the temperature drops from 1,050 °C to 950 °C, the orange area shrinks dramatically (Fig. 3b,c). It is worth noting that the contents of AlF, O and Ca in the generated magnesium vapour (Supplementary Note 7) and the temperature of the gradient cooling zone (Supplementary Fig. 3a) fluctuate frequently under industrial production conditions. These variations can cause fluctuations in the formation of $Ca_{12}Al_{14}F_2O_{32}$ (Supplementary Fig. 6d), thereby resulting in variations in the aluminium impurity content of the final magnesium product. Moreover, it is interesting to note that at high temperatures (Fig. 3a,b), $Ca_{12}Al_{14}F_2O_{32}$ is always prone to form when the molar ratio of Ca to O is 1:1 (red dashed line), regardless of the molar percentage of AlF. Considering that the content and proportion of Ca and O in the magnesium vapour are both difficult to control, it can be speculated that the use of solid calcium oxide (CaO) may have a strong and stabilizing absorption effect on AlF in the high-temperature zone, thereby effectively reducing the aluminium impurities.

Validation of the proposed impurity removal mechanism by experiments

To experimentally verify the predicted effect of CaO on removing Al impurities from the flowing magnesium vapour generated during the silicothermic reduction process, a miniature apparatus was

https://doi.org/10.1038/s41563-026-02561-2

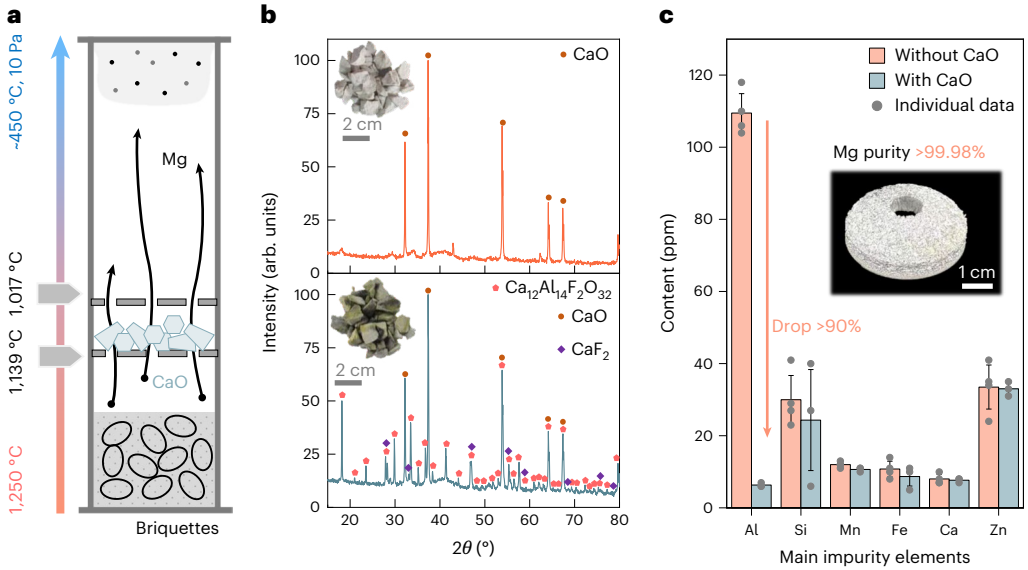


Fig. 4 | Comparative experiments showing the aluminium removal capability of CaO. a, Schematic of the silicothermic reduction process, showing a high-temperature reaction zone, gradient cooling zone and crystallization zone. The control setup was conducted without CaO, whereas CaO was introduced in the experimental groups within the temperature range of 1,139–1,017 °C. **b**, Morphological and phase analysis of CaO before and after use. CaO changes colour from white to yellowish black after use, whereas its overall morphology remains preserved. XRD patterns confirm the formation of $Ca_{12}Al_{14}F_2O_{32}$ and CaF_2 phases in the used CaO. **c**, Impurity content in the produced magnesium with and without using CaO. Each dot represents one independent experiment (without CaO, $n = 4$; with CaO, $n = 3$). Bars indicate mean values ± s.d. Aluminium content decreases markedly from 109.5 ppm to 6.3 ppm, demonstrating a reduction of over 90%. Other major impurities (Si, Mn, Fe, Ca and Zn) show no notable increase, with magnesium purity exceeding 99.98%.

constructed containing the key part of an industrial silicothermic reduction retort (Fig. 4a). To ensure the uniform placement of CaO and facilitate an even passage of magnesium vapour, the apparatus was set up vertically. Briquettes used for the silicothermic reduction reaction were sourced from an industrial plant, and CaO blocks of >95% purity and diameters of 10–20 mm were selected for this study. Before the experiment, the inner temperatures along the axial direction of the apparatus were measured carefully after the setting temperature reached a steady state. Approximately 250 g of briquettes were placed in the ~1,250 °C reaction zone to generate magnesium vapour, and ~20 g of CaO blocks were positioned in the region in which the temperature ranged from 1,139 to 1,017 °C. This temperature range in which CaO was introduced coincides with the temperature window where the thermodynamic formation probability of $Ca_{12}Al_{14}F_2O_{32}$ is the highest (Fig. 3) and majority of the $Ca_{12}Al_{14}F_2O_{32}$ compound was found in the industrial retort (Supplementary Fig. 3).

After the experiment, the colour of the CaO blocks was changed from white to a brownish appearance (Fig. 4b). The surface micromorphology of CaO was transformed from a relatively uniform granular structure with diameters of 1–2 μm to a larger, more irregular structure (Supplementary Fig. 7), indicating a chemical reaction rather than simple dust accumulation. XRD analysis confirmed that the reacted CaO displayed characteristic diffraction peaks of $Ca_{12}Al_{14}F_2O_{32}$ (Fig. 4b), providing strong evidence for the expected chemical reaction during the purification process. Purity analysis (Fig. 4c) on the final crystalline magnesium demonstrated that the average aluminium content in magnesium reached 6.3 ppm ± 0.5 ppm, an extremely low level compared with those in real industrial conditions. For comparison, experiments under exactly the same conditions but without using CaO were also carried out. The average aluminium content in magnesium was 109.5 ppm ± 5.4 ppm. This demonstrated that CaO had an excellent effect on removing aluminium impurities from magnesium, with an aluminium removal rate exceeding 90%. Additional experimental settings confirmed that the specific reaction mechanism involved CaO reacting with AlF to form $Ca_{12}Al_{14}F_2O_{32}$, along with Ca and CaF_2 as byproducts, and these byproducts did not contaminate the crystallized magnesium (Supplementary Note 8). As shown in Fig. 4c, the levels of Ca and other impurities did not increase and were even slightly reduced, resulting in magnesium with an overall purity exceeding 99.98% (Supplementary Table 7). Our experiments demonstrate that CaO is indeed an excellent medium that can be used to remove aluminium impurities from the flowing magnesium vapour.

Industrial-scale application and its effectiveness

For industrial application, an effective purification strategy must balance the impurity removal efficiency with system compatibility, environmental sustainability and cost. The impurity removal medium must neither introduce new impurities nor compromise the retort lifetime under operating conditions. Additionally, it should be readily accessible, inexpensive and recyclable. Calcined dolomite meets these requirements. It contains over 50 wt% of CaO as the active component for aluminium capture and is a primary raw material in magnesium production. It is both inexpensive and readily available on-site. It also remains chemically stable in the retort without generating negative effects on the retort (Supplementary Note 10). Moreover, the used CaO·MgO can potentially be used as a raw material in the next batch, enabling a closed-loop utilization within the process.

Besides material selection, another key concern for industrial scaling is the potential impact on magnesium yield, as the packed removal medium may hinder the smooth flow of magnesium vapour when the mass flow is substantially increased in industry. To mitigate this risk, two design strategies were implemented. First, the medium-to-briquette ratio was adjusted to a lower level sufficient to achieve effective purification without noticeably hindering vapour flow (for example, from 20 g:250 g in laboratory experiments to 500 g:250,000 g in industrial trials in this work). Second, as demonstrated in our previous work[42], the temperature in the silicothermic reduction retort gradually decreases from the reaction region towards the crystallization zone. Once the temperature of briquettes near the crystallization zone drops below ~1,050 °C, their reduction becomes insufficient, with reduction rates typically falling below 50%. Placing a removal medium in this region can serve as a thermal barrier, reducing heat loss from the reaction

https://doi.org/10.1038/s41563-026-02561-2

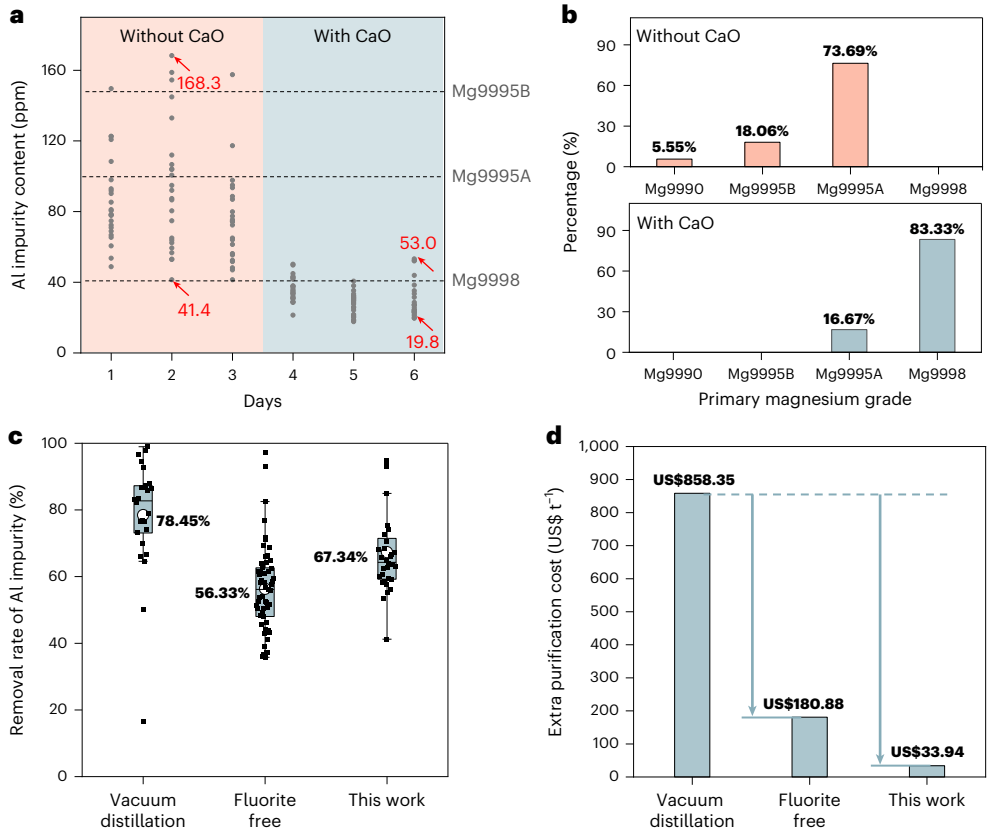


Fig. 5 | Industrial application of CaO for aluminium impurity removal and the overwhelming advantages compared with other methods. a, Aluminium impurity content without and with CaO·MgO (a common and ultra-cheap raw material in magnesium factories) in 6 days. Without CaO, the impurity levels fluctuate between 41.4 and 168.3 ppm, whereas with CaO, levels stabilize at 19.8–53.0 ppm. **b**, Distribution of primary magnesium grades before and after using CaO. Without the use of CaO, 73% of the magnesium ingots have aluminium content that meets the Mg9995A standard, and none meet the Mg9998 standard. By contrast, with CaO, over 83% of the magnesium ingots meet the high-purity Mg9998 standard for aluminium content. **c**, Comparison of aluminium impurity removal efficiency of different approaches. Each dot represents one independent experiment (vacuum distillation, $n = 26$; fluorite-free method, $n = 55$; this work, $n = 32$). The box plots display the median (central line), mean (white circle) and interquartile range, with the upper whiskers extending to the largest value ≤1.5× the interquartile range from the 75th percentile and the lower whiskers extending to the smallest value ≤1.5× the interquartile range from the 25th percentile. The proposed method achieves a mean removal efficiency of ~67.34%, higher than that of the fluorite-free method (56.33%) and equivalent to 86% of that of vacuum distillation (78.45%). **d**, Cost comparison of different purification methods. Our method is highly cost-effective, only increasing US$33.94 t^{-1} of magnesium for purification, approximately 20% of the fluorite-free method (US$180.88 t^{-1}) and 4% of vacuum distillation (US$858.35 t^{-1}). Details are provided in Supplementary Note 13.

zone to the crystallization zone and consequently elevating the local temperature. This allows a more complete reaction of briquettes, thereby achieving a higher magnesium yield. These factors together were expected to offset the modest increase in flow resistance, resulting in no noticeable loss of magnesium yield.

Industrial trials in a 30,000 t yr^{-1} magnesium plant confirmed the effectiveness of CaO·MgO in aluminium removal. CaO·MgO was used as a single-use removal medium in each production cycle, primarily due to its extremely low cost, on-site availability and straightforward integration into the existing process. As shown in Fig. 5a, aluminium impurity levels for each production day are represented by a column of data points, with each point corresponding to an ~2-t batch. Before applying the removal medium, aluminium impurity contents fluctuated widely between 41.1 and 168.3 ppm, with an average of 85.07 ppm (95% confidence interval, 78.10–92.03; standard deviation (s.d.), 29.64 ppm). By contrast, after introducing the removal medium, the average content dropped to 31.34 ppm (95% confidence interval: 29.29–33.40; s.d.: 8.74 ppm), with fluctuations narrowed to 19.8–53.0 ppm. Welch's analysis of variance confirmed that this reduction was statistically significant and not due to random variation (Supplementary Note 11). This decrease can sufficiently upgrade the product. Over three consecutive production days, the aluminium impurity levels in all batches met or exceeded the Mg9995A standard, the proportion meeting the Mg9998 standard rose from 0% to 83.3%, and the lowest grade improved from Mg9990 to Mg9995A (Fig. 5b). Importantly, purification was achieved without a noticeable impact on yield (Supplementary Fig. 11b): over the same 3-day production period (~100 t of magnesium per day), batches with CaO·MgO yielded an average of 39.15 kg magnesium per 250 kg briquette (per production unit), very close to 38.82 kg in the controls, with the difference well within the typical industrial fluctuation in yield. Moreover, the used CaO·MgO could be recycled by blending into fresh raw materials without a detectable influence on either the product quality or yield in subsequent production days (Supplementary Note 12). On the basis of these findings, the method—termed the CaO absorption method—was rapidly adopted across the plant, underscoring its industrial feasibility, simplicity and scalability.

Discussion

Techno-economic assessment highlights the clear advantages of the CaO absorption method over existing purification techniques, such as vacuum distillation and fluorite-free approaches. As shown in Fig. 5c, even at a substantially lower medium-to-briquette ratio in industrial trials (~500 g:250,000 g) compared with laboratory-scale tests (~20 g:250 g), the aluminium removal efficiency in industry

remained ~67.34%, higher than that of the fluorite-free method (56.33%) and lower than that of the vacuum distillation method (78.45%). The reduced efficiency relative to that of laboratory tests (>90%) can be partly attributed to the lower medium-to-briquette ratio and partly to differences in kinetic conditions between industrial and laboratory settings. Nevertheless, its cost and energy efficiency are outstanding. The extra purification cost relative to the traditional silicothermic reduction process is only ~US$33.94 t^{-1} of magnesium—just ~20% of the fluorite-free method (after accounting for yield loss) and ~4% of vacuum distillation (Fig. 5d and Supplementary Note 13). In particular, the plant in which the experiments were conducted represents a benchmark enterprise in magnesium industry, with typical industrial-scale capacities of 30,000 t yr^{-1} of silicothermic magnesium and 500 t yr^{-1} of vacuum-distilled magnesium production. Complementary throughput-independent energy analyses further confirmed the advantages, showing that the CaO absorption method requires only ~1.4% of additional energy consumed by vacuum distillation (Supplementary Note 13). Considering the substantial reduction in aluminium impurity levels (Fig. 5a,b) and the corresponding improvement in product value for higher-grade magnesium (Fig. 1b), the CaO absorption method delivers remarkable economic benefits, yielding an additional net profit of ~US$1,400 t^{-1} of magnesium.

This work also establishes a generalizable framework for impurity removal: by analysing vapour-phase impurity species and their associated deposits, one can reverse-engineer selective and system-compatible removal media. The spontaneous formation of such deposits under process conditions indicates that impurities prefer to stabilize within these phases, ensuring the selectivity and effectiveness of the designed media. Since the key elements forming these deposits are already present in the system, the resulting media are easily accessible and inherently compatible with the system. Similar strategies have also proven effective in decreasing Mn and Pb impurities in magnesium (Supplementary Note 14). Moreover, because interatomic interactions are the weakest in the gaseous state, it is easier and more effective to exploit the intrinsic physical and chemical properties of impurities to drive their preferential condensation or absorption on suitable media. This principle is applicable not only to magnesium but also to other metals with low melting points and high vapour pressures such as calcium and zinc.

In summary, this work addresses a long-standing industrial challenge: reducing both content and fluctuations of aluminium impurity in primary magnesium in a cost-effective way. Unlike traditional post-production purification, our strategy removes aluminium impurities directly during the reduction stage, by stabilizing aluminium as $Ca_{12}Al_{14}F_2O_{32}$ deposits ahead of magnesium condensation. Validated at the full industrial scale, this CaO-based method delivers superior cost-effectiveness and enables the large-scale production of low-Al magnesium for demanding applications such as electronic-grade titanium, nuclear-grade zirconium and biodegradable implants. Our methodological framework is not only applicable to other impurities in magnesium but also provides broader insights into purification strategies for vapour-phase metallurgical systems besides magnesium, thereby establishing a general approach for impurity control.

Online content

Any methods, additional references, Nature Portfolio reporting summaries, source data, extended data, supplementary information, acknowledgements, peer review information; details of author contributions and competing interests; and statements of data and code availability are available at https://doi.org/10.1038/s41563-026-02561-2.

References

1. Pollock, T. M. Weight loss with magnesium alloys. *Science* **328**, 986–987 (2010).
2. Prasad, S. S. et al. The role and significance of magnesium in modern day research—a review. *J. Magnes. Alloys* **10**, 1–61 (2022).
3. Chen, G. Z., Fray, D. J. & Farthing, T. W. Direct electrochemical reduction of titanium dioxide to titanium in molten calcium chloride. *Nature* **407**, 361–364 (2000).
4. Froes, F. H. *Titanium: Physical Metallurgy, Processing, and Applications* (ASM International, 2015).
5. US Geological Survey. *Mineral Commodity Summaries 2020* (US Geological Survey, 2020); http://www.usgs.gov/publications/mineral-commodity-summaries-2023
6. Fu, D. et al. Review on the silicothermic process for primary magnesium production. *Metall. Mater. Trans. B* **54**, 1–21 (2023).
7. Yang, B., Liu, B. Y., Yang, H. & Shan, Z. W. Brief analysis of the importance of high-purity raw materials: taking magnesium as an example. *Mater. China* **39**, 576–584 (2020).
8. Li, X. Caution on trace impurities. *Nat. Mater.* **22**, 402–403 (2023).
9. Yang, B., Zheng, R., Wu, G., Chang, Z. & Shan, Z. Minimizing pest aluminum in magnesium for the production of high-purity titanium. *J. Magnes. Alloys* **11**, 4189–4196 (2023).
10. Stephens, W. W. *Extractive Metallurgy of Zirconium—1945 to the Present* (ASTM International, 1984).
11. Yuan, T. C., Weng, Q. G., Zhou, Z. H., Li, J. & He, Y. H. Preparation of high-purity titanium by molten-salt electrolysis process. *Adv. Mater. Res.* **284–286**, 1477–1482 (2011).
12. Weng, Q., Li, R., Yuan, T., Jian, L. I. & He, Y. Valence states, impurities and electrocrystallization behaviors during molten salt electrorefining for preparation of high-purity titanium powder from sponge titanium. *Trans. Nonferrous Met. Soc. China* **24**, 553–560 (2014).
13. Vutova, K. et al. Investigation of electron beam melting and refining of titanium and tantalum scrap. *J. Mater. Process. Technol.* **210**, 1089–1094 (2010).
14. Ningbo Chuangrun New Materials. 3N-level high-purity sponge titanium. *CRNMC* http://www.crnmc.cn/product/high-purity-titanium-sponge/3n-grade-high-purity-titanium-sponge.html (2025).
15. Duo, Y. X., Wang, L. J., Li, Y. & Wei, Z. Z. Source analysis and control technology of impurity Al in titanium sponge. *Iron Steel Vanadium Titanium* **43**, 36–39 (2022).
16. Li, K. et al. Identification of source and control of oxygen and nitrogen impurities in Kroll process for preparation of ultra-soft titanium sponge. *J. Mater. Res. Technol.* **36**, 3104–3111 (2025).
17. Gadiyar, H. S. *Effect of Impurity Elements Al, Mn, and N_2 on the Corrosion Resistance of Zircaloy-2 in High Temperature Water and Steam* Report No. BARC-948 (Bhabha Atomic Research Centre, 1978).
18. Krishnan, R. & Asundi, M. K. Zirconium alloys in nuclear technology. *Proc. Indian Acad. Sci. (Engg. Sci.)* **4**, 41–56 (1981).
19. Nikulina, A. V. & Malgin, A. G. Impurities and their effect on the structure and properties of zirconium parts in nuclear reactors. *At. Energy* **105**, 328–339 (2008).
20. Witte, F. The history of biodegradable magnesium implants: a review. *Acta Biomater.* **6**, 1680–1692 (2010).
21. Gu, X. N. & Zheng, Y. F. A review on magnesium alloys as biodegradable materials. *Front. Mater. Sci. China* **4**, 111–115 (2010).
22. Sun, Y. et al. Translational status of biomedical Mg devices in China. *Bioact. Mater.* **4**, 358–365 (2019).
23. Li, C. et al. Design of biodegradable, implantable devices towards clinical translation. *Nat. Rev. Mater.* **5**, 61–81 (2020).
24. Ferreira, P. C., Piai, K. D. A., Takayanagui, A. M. M. & Segura-Muñoz, S. I. Aluminum as a risk factor for Alzheimer's disease. *Rev. Lat. Am. Enferm.* **16**, 151–157 (2008).
25. Sun, M. et al. Recent advances in the grain refinement effects of Zr on Mg alloys: a review. *Metals* **12**, 1388 (2022).
26. Balasubramani, N., Wang, G., StJohn, D. H. & Dargusch, M. S. The poisoning effect of Al and Be on Mg-1 wt.% Zr alloy and the role of ultrasonic treatment on grain refinement. *Front. Mater.* **6**, 322 (2019).

27. Abdellatif, M. Refining testwork on crude magnesium produced in the Mintek thermal magnesium process. In *Southern African Pyrometallurgy 2006* (ed. Jones, R. T.) 5–8 (Southern African Institute of Mining and Metallurgy, 2006).
28. Bowman, K. Magnesium by the magnetherm process: process contamination and fused salt refining. In *Light Metals 1986* (ed. TMS) 1033–1038 (The Minerals, Metals & Materials Society, 1986).
29. Cao, H. et al. Research status and prospects of melt refining and purification technology of magnesium alloys. *J. Magnes. Alloys* **7**, 370–380 (2019).
30. Revel, G., Pastol, J., Rouchaud, J. & Fromageau, R. Purification of magnesium by vacuum distillation. *Metall. Trans. B* **9**, 665–672 (1978).
31. Liang, D. et al. One-step preparation of high purity magnesium by vacuum distillation technology. *Vacuum* **192**, 110464 (2021).
32. Tian, Y. et al. Technical research on vacuum distillation to purify magnesium to 99.99% purity. *Mater. Res. Express* **8**, 56506 (2021).
33. Xiong, N. et al. The separation behavior of impurities in the purification of high-purity magnesium via vacuum distillation. *J. Sust. Metall.* **8**, 1561–1572 (2022).
34. Wulandari, W., Rhamdhani, A., Brooks, G. & Monaghan, B. J. Distribution of impurities in magnesium via silicothermic reduction. In *Proc. 5th European Metallurgical Conference (EMC 2009)* 1401–1415 (GDMB, 2009).
35. Toguri, J. M. & Pidgeon, L. M. High-temperature studies of metallurgical processes: part II. The thermal reduction of calcined dolomite with silicon. *Can. J. Chem.* **40**, 1769–1776 (1962).
36. Wang, C., Zhang, C., Zhang, S. J. & Guo, L. J. The effect of CaF_2 on the magnesium production with silicothermal process. *Int. J. Miner. Process.* **142**, 147–153 (2015).
37. Bobrov, Y. P. et al. Obtaining of high purity magnesium. *Vopr. At. Nauki Tekh.* **101**, 17–20 (2016).
38. Xu, J. et al. Mechanism of slag pellets sticking on the wall of reduction pot in magnesium production by Pidgeon process. *J. Magnes. Alloys* **12**, 2397–2412 (2024).
39. Demiray, Y. & Yücel, O. Production and refining of magnesium metal from Turkey originating dolomite. *J. Metall. Eng.* **31**, 251–257 (2012).
40. Wynnyckyj, J. R. & Pidgeon, L. M. Equilibria in the silicothermic reduction of calcined dolomite. *Metall. Trans.* **2**, 979–986 (1971).
41. Toguri, J. M. & Pidgeon, L. M. High-temperature studies of metallurgical processes: part I. The thermal reduction of magnesium oxide with silicon. *Can. J. Chem.* **39**, 540–547 (1961).
42. Zheng, R. et al. Principle exploration and application of simultaneous achieving production and quality of magnesium in silicothermic reduction process. *Chin. J. Nonferrous Met.* **33**, 2347–2355 (2023).

Publisher's note Springer Nature remains neutral with regard to jurisdictional claims in published maps and institutional affiliations.

Springer Nature or its licensor (e.g. a society or other partner) holds exclusive rights to this article under a publishing agreement with the author(s) or other rightsholder(s); author self-archiving of the accepted manuscript version of this article is solely governed by the terms of such publishing agreement and applicable law.

© The Author(s), under exclusive licence to Springer Nature Limited 2026

Methods

Quasi-in situ collection of natural deposits

Collecting deposits from the inner walls of the retort within the gradient cooling zone and accurately correlating them with specific locations and temperatures presented great challenges. To overcome this, we lined the interior of the retort with steel plates matching its length. After high-temperature operation, the retort was removed from the furnace and allowed to cool naturally. The differences in thermal expansion between the retort material and the attached deposits caused the deposits to detach and fall onto the corresponding steel plates. By carefully removing the steel plates horizontally from the retort, we were able to observe the detached deposits that had adhered to the retort's inner wall and pinpoint their exact locations.

To correlate the locations of the deposits with temperature, the temperature was measured along the retort at 100-mm intervals, starting from the weld seam between the retort and the crystallizer, extending through the gradient cooling zone and into the high-temperature zone. This measurement procedure was repeated across three retorts to ensure measurement accuracy and reproducibility.

Thermodynamic analysis

The ternary phase diagram of the AlF–Ca–O system was calculated using the Phase Diagram module of the commercial thermodynamic software FactSage 7.3 (ref. 43). Calculations were performed at a pressure of 10 Pa and temperatures of 1,150 °C, 1,050 °C, 950 °C and 750 °C. The molar ratios of AlF/(AlF+Ca+O) and O/(AlF+Ca+O) were varied between 0 and 1 to maintain a correlation between the concentrations of AlF, Ca and O, and to ensure that all components were included within the 0–1-mol range. The databases used for these calculations included FactPS, which contains thermodynamic data for pure substances relevant to the silicothermic reduction process. Before performing the analysis, we assessed the potential discrepancies between databases (FactPS alone versus FactPS combined with FToxid and FTsalt, which provides broader coverage of oxides, salts and their solutions). As the deviations were negligible and the phase evolution trends remained consistent (Supplementary Note 6), FactPS was adopted as the primary database to maximize computational efficiency.

Settings of confirmatory comparative experiments

Comparative experiments were conducted to verify the aluminium impurity removal efficiency of CaO using a self-designed apparatus. For each experiment, the temperature in the high-temperature reaction zone was set at 1,250 °C, whereas the temperature in the low-temperature crystallization zone was maintained at 450 °C, with a pressure of 10–100 Pa in the crystallization zone. Temperature measurements were taken at 50-mm intervals along the apparatus, from the high-temperature reaction zone to the low-temperature crystallization zone.

In the control group, approximately 250 g of briquettes (provided by Taida Coal Chemical) were placed in the high-temperature reaction zone. The temperature was ~1,250 °C, and the reaction lasted for 2 h. In the experimental group, in addition to the above conditions, CaO blocks (equivalent diameter of 10–20 mm and 20 g per run) were placed in the 1,139–1,017 °C region. Each set of experiments was repeated at least three times to ensure the reliability and accuracy of results.

Industrial experiments were carried out at a magnesium plant with an annual capacity of 30,000 t. Each reduction retort was charged with ~250 kg of briquettes together with ~500 g of CaO·MgO. The silicothermic reduction process was conducted at 1,250–1,280 °C under an ~10-Pa vacuum. The composition of CaO·MgO used as the removal medium is provided in Supplementary Table 14.

Microstructure, composition and purity analysis

The phases of the collected industrial deposits, as well as CaO before and after use, were characterized using XRD with a D8 ADVANCE A25 diffractometer. The analysis was conducted with a Cu target at a tube voltage of 40 kV and a tube current of 40 mA. The diffraction angle ranged from 10° to 80° (2θ), with a scan speed of 7° min^{-1}.

The micromorphology and composition of the industrial deposits and CaO were examined using scanning electron microscopy (SEM; Hitachi SU8230) equipped with energy-dispersive X-ray spectroscopy (Bruker XFlash 6|60). SEM imaging and energy-dispersive X-ray spectroscopy analysis were performed at an accelerating voltage of 10 kV and a beam current of 10 μA.

To analyse the purity of magnesium, the crystalline product was first remelted to homogenize impurity distribution, and the resulting cast ingot was characterized at multiple points using spark optical emission spectroscopy (GNR S5). Before use, the instrument was calibrated and cross-validated against both certified reference materials (G315, G311, RMG11-38 and E4131B) and in-house samples quantified by inductively coupled plasma mass spectrometry (Supplementary Note 16). The average impurity concentrations and standard deviations were calculated to assess both impurity levels and their fluctuation. For industrial-scale trials, 95% confidence intervals and Welch's analysis of variance were additionally applied to evaluate the reliability of the impurity results and the statistical significance of the purification effect.

Data availability

The data supporting the findings of this study are available within the article and its Supplementary Information. Additional data are available from the corresponding author upon reasonable request. Source data are provided with this paper.

References

43. Bale, C. W. et al. FactSage thermochemical software and databases, 2010–2016. *Calphad* **54**, 35–53 (2016).

Acknowledgements

This work was supported by the National Natural Science Foundation of China (U24A2021 to Z.-W.S.; 523B2001 to R.Z.; 52031011 to Z.-W.S.), the Science and Technology Department of Shaanxi Province (2023GXLH-029 to Z.-W.S.), the Innovation Capability Support Program of Shaanxi (2023ZSJD-05 to Z.-W.S.) and the Yulin Municipal Science and Technology Bureau (2023-CXY-199 to Z.-W.S.). We thank X.-W. Zhu (School of Humanities and Social Sciences, Xi'an Jiaotong University), X.-B. Hao, Z.-K. Wang, A. Wang, X.-F. Zhang, Y.-Z. Ma, X.-H. Cheng, C.-W. Fan and Y.-J. Zhang (School of Materials Science and Engineering, Xi'an Jiaotong University) for assistance in this work. We also thank Y.-L. Yang, W.-F. Wang, Z.-J. Gao and M.-H. Lu (Fugu TaiDa Coal Chemical) for providing the chemical composition data of raw materials and primary magnesium, and for facilitating the industrial experimental conditions.

Author contributions

Z.-W.S. designed and supervised the project. R.Z. and B.Y. performed the background investigation. R.Z. conducted the thermodynamic calculations, performed the experiments and analysed the data. R.Z. and W.-Y.Y. characterized the deposits using XRD, SEM, energy-dispersive X-ray spectroscopy and optical emission spectroscopy. R.Z., Y.-C.W., B.-Y.L. and Z.-W.S. wrote the paper. All authors contributed to the discussion and interpretation of the data.

Competing interests

The authors declare no competing interests.

Additional information

Supplementary information The online version contains supplementary material available at https://doi.org/10.1038/s41563-026-02561-2.

Correspondence and requests for materials should be addressed to Zhi-Wei Shan.

Peer review information *Nature Materials* thanks Gisele Azimi, Semiramis Friedrich and the other, anonymous, reviewer(s) for their contribution to the peer review of this work.

Reprints and permissions information is available at www.nature.com/reprints.